

# Phonon and magnon jets above the critical current in nanowires with planar domain walls

Maria Stamenova,<sup>1,\*</sup> Plamen Stamenov,<sup>1</sup> and Tchavdar Todorov<sup>2</sup>

<sup>1</sup>*School of Physics and CRANN, Trinity College, Dublin 2, Ireland*

<sup>2</sup>*Centre for Quantum Materials and Technologies, Queen's University, Belfast, UK*

We show through non-equilibrium non-adiabatic electron-spin-lattice simulations that above a critical current in magnetic atomic wires with a narrow domain wall the electron flow triggers violent stimulated emission of phonons and magnons with an almost complete conversion of the incident electron momentum flux into a phonon and magnon flux. The electronic current suffers a heavy suppression above this threshold. This poses a fundamental limit to the current densities attainable in atomic wires. At the same time it opens up an exciting way of generating the alternative quasi-particle currents above once the requisite electronic-structure properties are met.

## I. INTRODUCTION

Electron-phonon scattering is how electrons and nuclei in solids maintain thermal equilibrium. Nanoscale devices allow enormous current densities leading to violent electron-phonon dynamics. The most familiar is Joule heating, driven by spontaneous phonon emission [1, 2]. For a long time it was considered a central stability-limiting mechanism for small conductors. However it is now becoming clear that stimulated processes can play an even bigger role. Two key effects that can be traced to these processes are electronic friction [3] and non-conservative current-induced forces and torques [4–6].

Current-induced magnetic domain wall (DW) motion through spin-transfer torques (STT), but also the interaction between magnetic texture and spin-waves (magnons), is instrumental for new spintronic logic and data-storage technologies. For instance DWs can act as waveguides for spin-waves, which transmit information without Joule losses [7]. Conversely, magnonic currents have been found to transfer angular momentum to DWs, similarly to STTs, resulting in their translational motion [8].

simulations coupling electronic, lattice and spin degrees of freedom, that stimulated phonon emission poses a fundamental limit on the currents that can be passed with impunity through electronic and spintronic devices. There is a critical current density of  $10^{12} - 10^{13} \text{ Am}^{-2}$ , above which the current generates violent phonon jets with an almost complete conversion of the electron momentum flux into phonon momentum flux. A related phenomenon occurs in magnetic structures with sharp non-collinear features – the emission of magnon jets as a result of the exchange interaction between the itinerant electrons and the spins in the DW. In both cases the emitted waves are nearly monochromatic with momentum of  $2k_F$  for phonons and  $|k_F^\uparrow - k_F^\downarrow|$  for magnons. Because these processes are stimulated, they are captured by the simplest form of non-adiabatic dynamics, Ehrenfest dynamics, which we have implemented in our open-boundary electron-phonon-spin simulations.

Next we outline our arguments and simulation method. Then we present the results and conclude with a summary and experimental challenges.

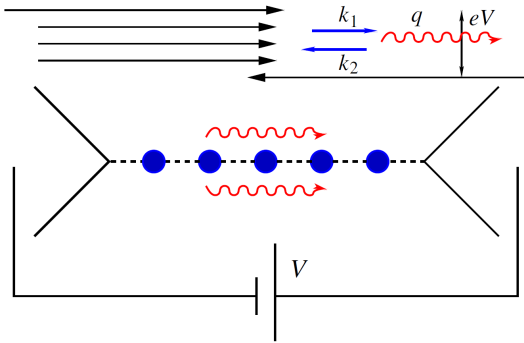


FIG. 1. (Color online) The uncompensated stimulated directional phonon emission process.

Here we show, through time-dependent open-boundary

## II. SPONTANEOUS AND STIMULATED PROCESSES

Consider a quantum harmonic oscillator coupled to electrons through the Hamiltonian

$$H = \sum_{\alpha} \epsilon_{\alpha} c_{\alpha}^{\dagger} c_{\alpha} - \sum_{\alpha, \beta} F_{\alpha \beta} \sqrt{\frac{\hbar}{2M\omega}} c_{\alpha}^{\dagger} c_{\beta} (a^{\dagger} + a) + \frac{\hbar\omega}{2} (a^{\dagger} a + a a^{\dagger}) \quad (1)$$

where all symbols have the usual meaning. Lowest-order time-dependent perturbation theory then gives for the rate of change of the oscillator energy  $E_{\text{osc}} = \hbar\omega \langle a^{\dagger} a + a a^{\dagger} \rangle / 2$

\* Contact email address: stamenom@tcd.ie

### III. METHODOLOGY

$$\begin{aligned} \dot{E} = & -\frac{2\pi}{\hbar} \frac{\hbar}{2M\omega} \left\{ E \sum_{\alpha,\beta} (f_\beta - f_\alpha) |F_{\alpha\beta}|^2 \delta(\epsilon_\beta - \epsilon_\alpha + \hbar\omega) \right. \\ & - \frac{\hbar\omega}{2} \sum_{\alpha,\beta} f_\alpha (1 - f_\beta) |F_{\alpha\beta}|^2 [\delta(\epsilon_\beta - \epsilon_\alpha + \hbar\omega) \\ & \left. + \delta(\epsilon_\beta - \epsilon_\alpha - \hbar\omega)] \right\} \end{aligned} \quad (2)$$

where  $f_\alpha = \langle c_\alpha^\dagger c_\alpha \rangle$ . The terms in the second line of Eq. [2] give the power into the oscillator from an effective corpuscular force noise [3] due to electrons, absent from Ehrenfest dynamics [9]. This noise drives spontaneous phonon emission.

The terms in the first line correspond to stimulated processes captured by Ehrenfest dynamics. Under normal conditions lower-lying electronic states are more highly populated and  $f_\beta > f_\alpha$ . Then the minus sign in front produces exponential damping of the oscillator energy. This is the familiar electronic friction [10, 11]. However if we excite the electrons sufficiently, the sign can flip, producing an explosive growth of the phonon population.

One such situation is an inverted electronic population [11, 12], resulting in the so-called negative friction [13]. Another is electronic transport, which involves the promotion of electrons from below the Fermi level to states of opposite velocity above the Fermi level. In Ref. 5 it is shown that the condition for the sign flip then is  $v_{\text{drift}} = c$  where the two velocities are the electron drift velocity and the speed of sound, respectively. It is shown also that this results in the exponential growth of forward-travelling phonons and that this is exactly equivalent to the effect of non-conservative current-induced forces [14–16].

The physics of this process is shown in Fig. 1. When the energy window for conduction  $eV_b$  exceeds  $\hbar\omega$  electrons can emit forward-travelling phonons and backscatter into a lower-energy state, while there are no electrons in the conduction window travelling the other way to reabsorb these phonons. The result is uncompensated stimulated forward phonon emission – the process we are interested in. The condition  $eV_b = \hbar\omega$  is equivalent to the earlier condition  $v_{\text{drift}} = c$  in 1D:

$$v_{\text{drift}} = \frac{eV_b}{\pi\hbar} \frac{\pi}{2k_F} = \frac{\omega}{q} = c \quad (3)$$

where we use quasi-momentum conservation  $q \sim 2k_F$  and assume dispersionless phonons for simplicity. The critical bias for the process  $eV_b \sim \hbar\omega$  is between 10s and 100s of meV, well in the nano-electronics experimental range. The corresponding current densities are  $10^{12} - 10^{13} \text{ Am}^{-2}$ .

The prediction is that above these current densities something catastrophic should happen in the atomic dynamics. This is the effect we set out to simulate, together with its analogue for magnons.

Our system is a 1D atomic wire of  $N = 300$  atoms [Fig. 1(a)]. The itinerant  $s$  electrons are described through a non-collinear spin-dependent tight-binding Hamiltonian with a single real-space basis state  $|i, s\rangle$  with two possible values of the spin label  $s = \pm 1$  per atom  $i$ ,

$$\begin{aligned} H_e = & \sum_{i,j,s} [(E_0 + U_C \Delta n_i) \delta_{ij} + t_{ij}(1 - \delta_{ij})] c_{is}^\dagger c_{js} \\ & - J_{sd} \sum_{i,s,s'} (\boldsymbol{\sigma}_{ss'} \cdot \mathbf{S}_i) c_{is}^\dagger c_{is'} \end{aligned} \quad (4)$$

where  $\Delta n_i = n_i - n_{0,i}$  is the excess onsite charge and  $\boldsymbol{\sigma}$  is the vector of Pauli spin matrices scaled by  $1/2$ . We explore a half-metallic regime with  $n_{0,i} = n_0 = 0.25 \text{ e/site}$  [see Fig. 1(c)]. Source (S) and a drain (D) regions are defined as 25-atom-long segments at each chain end. The central region (C) contains the remaining 250 atoms and only there the Coulomb interaction  $U_C$  is applied. Current-carrying conditions are imposed through a semi-empirical TD open-boundary method[17], based on a modified quantum Liouville equation for the electronic density matrix

$$\frac{\partial \hat{\rho}}{\partial t} = \frac{i}{\hbar} [\hat{\rho}, \hat{H}_V] - \Gamma (\hat{\rho} - \hat{\rho}_0) \quad (5)$$

where  $\Gamma$  is a real parameter and  $\hat{\rho}_0$  is such that

$$\rho_{0,ij}(t) = \begin{cases} \rho_{V,ij}(t=0) & \text{for } i, j \in \text{S, D} \\ \rho_{ij}(t) & \text{otherwise} \end{cases} \quad (6)$$

Bias of  $\pm V_b/2$  is applied to S/D [see Fig. 1(a)] at  $t = 0$  and  $\rho_V$  is the ground state of the biased Hamiltonian  $H_V = H_e - \sum_{i,j \in \text{S}} V_b/2 + \sum_{i,j \in \text{D}} V_b/2$ .

The classical degrees of freedom are a set of localised spins  $\{\mathbf{S}_i\}$ , one per site, and atomic positions  $\{\mathbf{R}_i\}$ . They are both propagated dynamically only in the C region, while in S/D they remain fixed. For the classical ( $d$ ) spins we integrate the Liouville equation

$$\frac{d\mathbf{S}_i}{dt} = \frac{1}{\hbar} (\mathbf{S}_i \times \mathbf{B}_i), \quad \text{where}$$

$$\mathbf{B}_i = J_{sd} \langle \boldsymbol{\sigma} \rangle_i + J_{dd} \sum_{j \neq i} \mathbf{S}_j e^{-\left(\frac{R_{ij}-a}{a}\right)} + 2J_z (\mathbf{S}_i \cdot \hat{\mathbf{z}}) \hat{\mathbf{z}}$$

is the effective magnetic field at site  $i$ . Here  $\langle \boldsymbol{\sigma} \rangle_i = \sum_{s,s'} \langle \hat{c}_{is}^\dagger \hat{c}_{is'} \rangle \boldsymbol{\sigma}_{ss'}$ . The classical ( $d$ ) spins  $|\mathbf{S}_i| = S = 1$  are locally exchange-coupled ( $J_{sd} > 0$ ) to the instantaneous expectation value of the itinerant ( $s$ ) electron spin, which gives rise to STT.  $\mathbf{S}_i$  are also coupled to their peers through a distance-dependent Heisenberg interaction with a strength  $J_{dd}$ , at the nearest-neighbour distance  $a$ , and  $J_z$  is an easy-axis anisotropy. The initial ( $t = 0$ ) configuration is obtained through a damped relaxation of  $\{\mathbf{S}_i\}$  such that a stationary planar (Néel) DW is formed along the easy  $z$ -axis [Fig. 2(a)].

At  $t = 0$  the chain is uniform with lattice spacing  $a$ . Atomic positions in C evolve according to

$$M\ddot{\mathbf{R}}_i = -2 \sum_{j \neq i} \Re(\rho_{ij}) \nabla_i t_{ij} - \sum_{j \neq i} \nabla_i [\Phi_{ij} - V_{S,ij}] \quad (7)$$

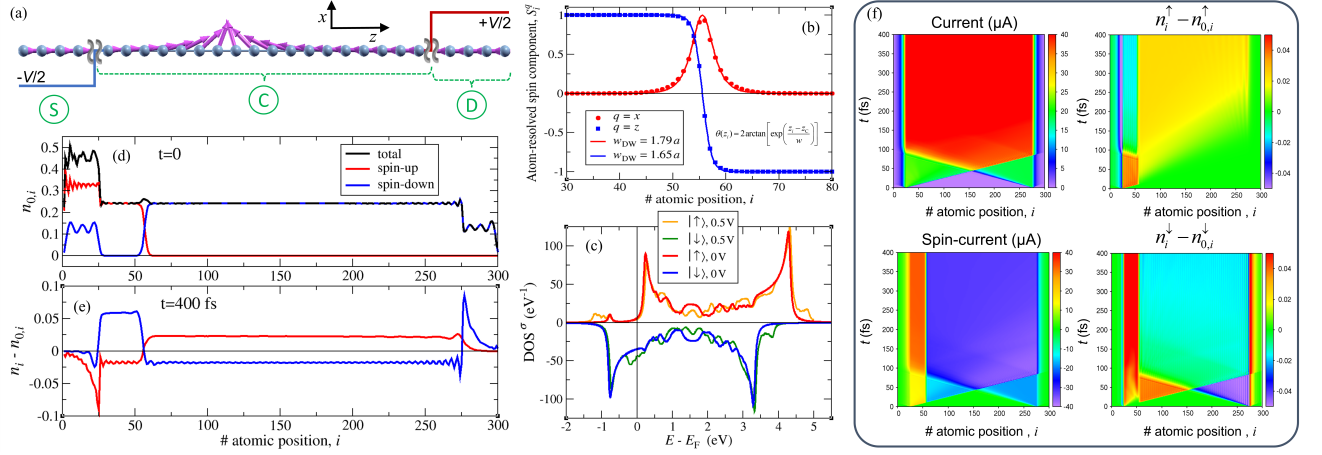


FIG. 2. (Color online) (a) Schematic of the relaxed planar DW formed by the classical spins in the chain at  $t = 0$ , showing the application of a potential drop to the ends of the chain ( $V_b > 0$ ). (b) In-plane components of the classical spins at  $t = 0$  and fits to the analytical profile from the 1D anisotropic Heisenberg model. (c) Self-consistent DOS at  $t = 0$  with respect to the two in-plane quantisation axes. (d,e) Spin-density distribution at  $t = 0$  and  $t = 100$  fs, respectively. (f) Heat maps over space and time of indicated early-dynamic properties at  $V_b = 1$  V: (left column) charge and spin-polarized current; (right column) variation of each spin-density with respect to the  $t = 0$  distribution [panel (d)].

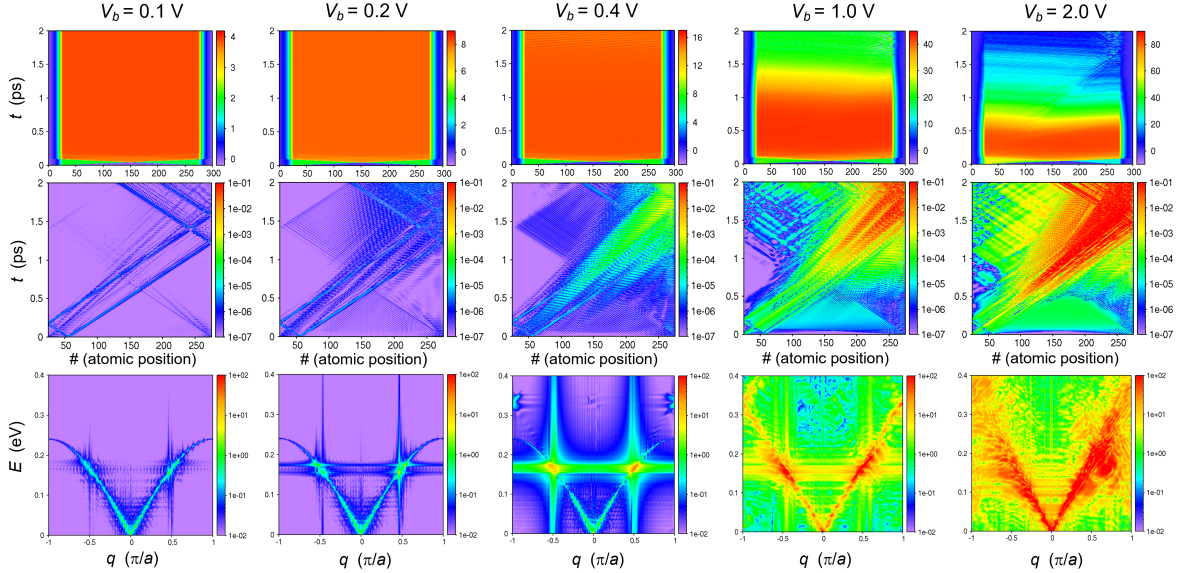


FIG. 3. (Color online) Dynamics with frozen spins: heatmap plots in columns for given applied bias voltage (between 0.1 and 2 V). The first two rows depict the real-space and time evolution of the bond currents (in  $\mu\text{A}$ ) and the kinetic energy of the atoms (in eV), respectively. In the bottom row are the corresponding 2D-Fourier-transform images of the atomic velocities.

where we define the distance dependence of the hopping parameter  $t_{ij}$ , the pair potential  $\Phi_{ij}$  and the classical spin interaction  $V_{S,ij}$ , respectively, as

$$t_{ij} = -\frac{\epsilon C}{2} \left( \frac{a_f}{R_{ij}} \right)^q, \quad \Phi_{ij} = \epsilon \left( \frac{a_f}{R_{ij}} \right)^p, \quad (8)$$

$$V_{S,ij} = -J_{dd} \exp \left( -\frac{R_{ij} - a}{a} \right) \mathbf{S}_i \cdot \mathbf{S}_j. \quad (9)$$

The parameters are:  $E_0 = 0$  eV,  $U_C = 1$  eV,  $J_{sd} = 1$  eV,  $J_{dd} = (20 - 200)$  meV,  $J_z = J_{dd}/2$ ,  $a = 2.5$  Å,  $M = 10$  amu,  $\epsilon = 7.868 \times 10^{-3}$  eV,  $a_f = 4.08$  Å,  $C = 31.16$

(such that  $t_{ij} = -1.0$  eV for nearest neighbours),  $q = 4$  and  $p = 11$  [18]. These parameters produce compressed chains [19] to suppress a Peierls distortion [19].

These equations of motion constitute Ehrenfest dynamics for our electron-phonon-magnon problem. Ehrenfest dynamics captures electronic friction, non-conservative forces and Berry forces in transport [9] but excludes electronic noise and spontaneous emission for phonons or spin noise for the magnetic degrees of freedom [20]. Our interest here is precisely in the stimulated processes that the mean-field Ehrenfest approximation is

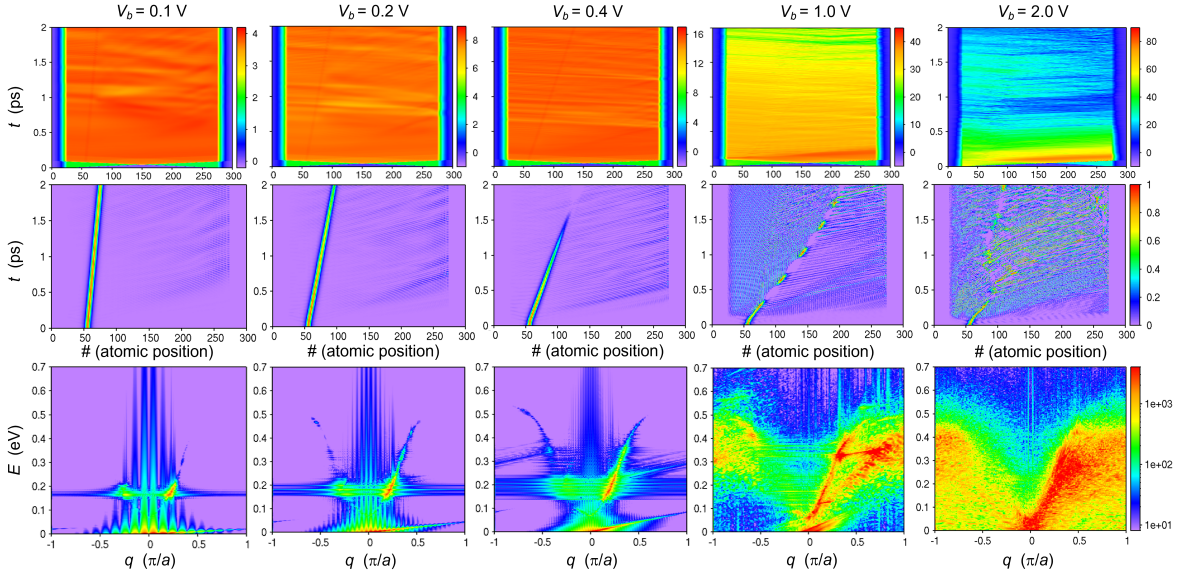


FIG. 4. (Color online) Dynamics with frozen atoms: heatmap plots in analogy with Fig. 3, here the rows from the top are the current (in  $\mu\text{A}$ ), the  $S^z$  component (in  $\hbar$ ) and the  $2\text{DFT}(S^x)$ . Here  $J_{dd} = 80$  meV,  $J_z = 40$  meV. Note that calculated magnon dispersions differ from a cosine as per the nearest-neighbour Heisenberg model, because of the long-range  $J_{dd}$  [see Eq. 8].

designed for.

The resultant electronic structure is shown in Fig. 2. The initial position of the DW (around atom #56) can be seen from the steps in the two spin populations in the initial statically polarised state described by  $\hat{\rho}_0$ , panel (c). Panel (e) shows that for the present parameters there is only one open spin channel. Indeed panel (e), which displays the evolution of the charge ( $I_i^\uparrow + I_i^\downarrow$ ) and the spin-polarised ( $I_i^\uparrow - I_i^\downarrow$ ) bond currents [21] under a bias of 1 V (with frozen atoms and frozen classical spins), shows currents (around  $38.5 \mu\text{A}$  at 1 V) corresponding to one spin channel.

#### IV. RESULTS AND DISCUSSION

We now apply a series of biases with moving ions and frozen magnetisations, Fig. 3. At about 0.4 V we see a dramatic blast on the panel showing the 2D-Fourier transform (2DFT) of the atomic velocities, while the atomic kinetic energies in the plots above clearly display the phonon jets. They first appear around 0.2 V. The phonon dispersion on the 2dFT plot shows that at a phonon wavevector  $q = 2k_F = \pi/2a$  the phonon frequency is in the region of 0.17 eV, corresponding to the activation bias.

These results demonstrate the effect: currents above the critical value generate explosive phonon fluxes and the current drops heavily as a result. Quasi-momentum balance requires the kinetic energy per atom at the right end to be  $\sim neV_b/2$  where  $n$  is the number of electron per atom. This gives a kinetic energy of about 0.1 eV at 1 V, in rough agreement with Fig. 3. Once the phonon

jet has been unleashed, the current drops to about the threshold value, around  $10 \mu\text{A}$  here, as is seen from Fig. 3 at 1 V and 2 V.

Notice also the approximately exponential growth of the phonon jet along its propagation. This is the tell-tale sign of the stimulated process and shows the key distinction from Joule heating.

We now consider the spin dynamics. Fig. 4 shows the magnetisation dynamics with frozen atoms at different biases. At small bias, the spin-polarised current drives DW motion. Notice the signature of the linear motion of the DW on the Fourier spectrum: the linear dispersion, most clearly seen at low bias. With increasing bias the quadratic magnon dispersion becomes visible with its lopsided population towards right-going magnons. However at and above 1 V the current drops while generating a dramatic magnonic population.

These effects define a magnonic analogue of the phonon jets. Similarly to the phonons, the magnons are emitted preferentially into right-travelling states with a given crystal momentum  $q$ , this time around  $\pi/4$  (see 2DFT panels for  $V_b \leq 0.4$  V in Fig. 4). These can be related to two processes involving momentum exchange with the current-carrying electrons. As  $|k_F^\uparrow - k_F^\downarrow| \approx \pi/4a$  (we are in a half-metallic regime with a minority spin wavevector approaching 0), where spin-up/down swap roles as majority/minority carriers across the DW, a majority spin traversing the wall non-adiabatically from left to right gives up crystal momentum of  $q = \pi/4a$  as it becomes a minority spin on the far side. We see evidence of such non-adiabatic wall-crossing in Fig. 2(f). The second mechanism is spin-flip scattering, key to the magnon-drag effect [22]. We see evidence for it in the suppression



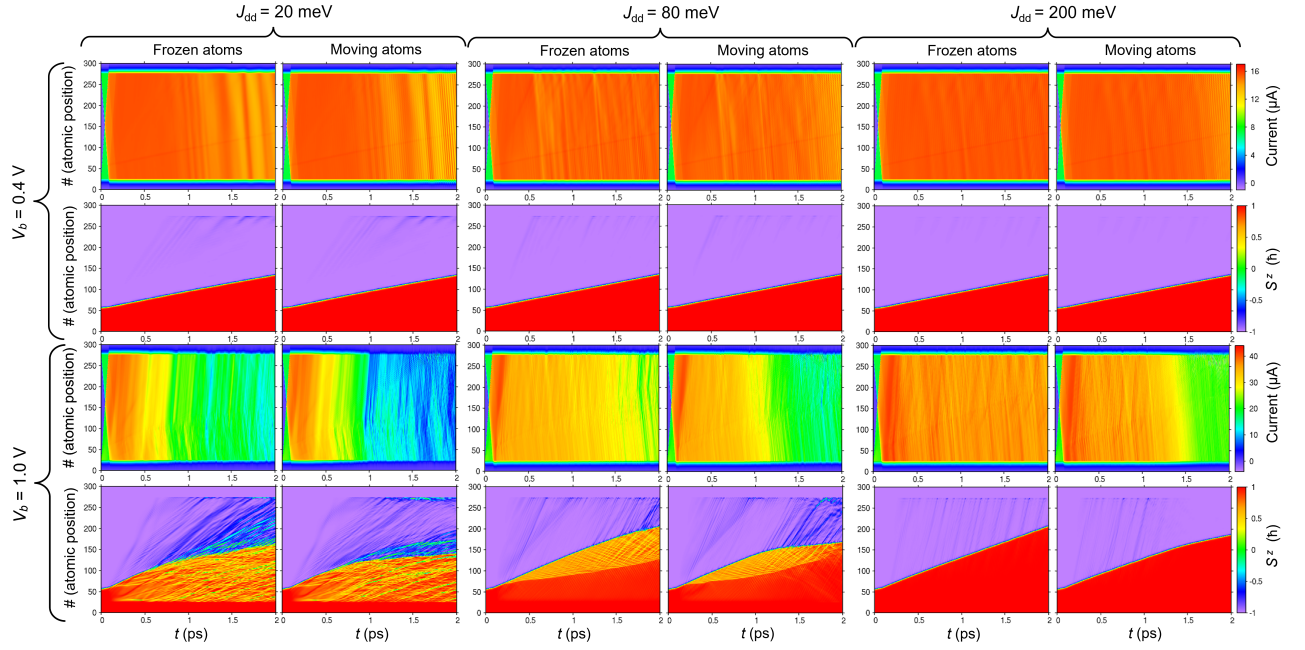


FIG. 5. (Color online) Heatmap plots [the usual  $(t - z)$  plane] in pairs of columns for each given value of  $J_{dd}$ : 'frozen' and 'moving' atoms; and pairs of rows showing the evolution of the bond currents (in  $\mu A$ ), followed by the  $S^z$  component for two bias voltages (as indicated on the left). Note that the anisotropy constant is  $J_z = J_{dd}/2$ .

of the current in Fig. 4 and Fig. 5, as well as the reduction of the DW speed below the adiabatic STT limit [23]: at  $V_b = 1$  V average  $V_{DW} \approx 89 a \text{ ps}^{-1}$ , while for the given average current of  $I = 34.0 \mu A$  in the first ps after the transient stage, the adiabatic STT speed [23] is  $aPI/(2eS) = 97 a \text{ ps}^{-1}$ , for a calculated spin-polarisation  $P = 91$  % of the current.

Between 1 and 2 V the DW velocity approaches the magnon group velocity (with an average of  $300 a \text{ ps}^{-1}$ , see 2dFTs on Fig. 4). For such voltages the DW disintegrates and leaves behind a trail of magnetic structures that propagate as solitons. Their signature on the dispersion is a linear trace through the origin. Therefore our DW cannot break the magnon speed barrier. This marks a second threshold effect, bearing an analogy with Cherenkov radiation or sonic boom, in the dynamics of the spintronic device.

Lastly, Fig. 5 examines the effect of the classical spin coupling  $J_{dd}$  and shows combined lattice-magnetisation dynamics. At low  $J_{dd}$  the magnon emission is more intense and blocks the DW motion early on due to the suppression of the current. This is suppressed at large  $J_{dd}$  because of the increased magnetic stiffness. Comparing the currents for frozen atoms with those for the combined dynamics shows that the phonon and magnon effects both contribute to the suppression of the current: the ideal current for 1 V in our case is about  $40 \mu A$ .

We thus witness not one but two superimposed mechanisms whereby increasing bias unleashes a transition from ballistic transport to a regime where the incident electron quasi-momentum flux becomes almost entirely con-

verted into a powerful phonon or magnon flux, or both, accompanied by a heavy suppression of the current. The phonon jet is associated with a clearcut threshold bias while in the magnon case the threshold is the breakdown of the DW as it approaches the magnon velocity.

This transition poses a fundamental limit to the current densities in electronic and spintronic devices. At the same time it opens up an exciting mechanism for producing coherent monochromatic, or nearly monochromatic, phonon beams that may generate novel applications. Notice that a single-frequency phonon current requires small bias: Fig. 3 shows how at large bias the violent dynamics splits the phonon frequency into a shower due to anharmonicity. Furthermore the DW acts as a source of magnon current: at low bias the magnonic excitations in Fig. 4 clearly originate from the DW due to the non-adiabatic spin propagation discussed earlier. This furnishes a coherent magnon source analogous to the phonon source above.

These predictions are our main finding. We now consider the experimental evidence. Above we assumed that  $k_F < \pi/2a$ . If  $k_F > \pi/2a$  then the emitted phonons with  $q = 2k_F$  fall beyond the zone boundary and will manifest as backward-travelling phonons by Umklapp scattering. At the transition between these two cases,  $k_F = \pi/2a$ , every emitted phonon lies on the zone boundary with  $q = \pi/a$  and equally qualifies as a back-travelling phonon with  $q = -\pi/a$  which can be reabsorbed by the current-carrying electrons in the reverse process. Then we still expect a suppression of the current but no pile-up in the phonon population. Both of these situations we have seen

in test simulations.

The boundary case was observed experimentally in Au atomic wires [24] and indeed long Au chains withstand high biases: 1 V or more. By contrast Pt whose Fermi properties are dominated by a partially filled d-band [25] shows very different behaviour and Pt chains fail at much lower biases [26]. We propose this as direct evidence for the phonon-jet effect, which shows that it is heavily material-dependent. Magnetic analogies could be sought at low temperatures and materials with heavy-magnon dispersions, opening up applications as magnon-current sources and techniques for the detection of DWs in magnetic nanostructures. These crucial dependencies on the

electronic structure will, we hope, stimulate lively theoretical and experimental work to detect and exploit these effects.

## V. ACKNOWLEDGEMENTS

We gratefully acknowledge funding from the Science Foundation Ireland: SFI Grants No. 18/SIRG/5515 and 18/NSFC/MANIAC. We thank the Irish Centre for High-End Computing (ICHEC) and the Trinity Research IT Centre (TCHPC) for the provision of computational facilities and support. We thank Andrew Horsfield, Myrta Grüning and Ray McQuaid for helpful discussions.

- 
- [1] T. N. Todorov, *Phyl. Mag. B* **77**, 965 (1998).
  - [2] T. Frederiksen, M. Brandbyge, N. Lorente, and A. P. Jauho, *Phys. Rev. Lett.* **93**, 256601 (2004).
  - [3] J.-T. Lü, M. Brandbyge, P. Hedegård, T. N. Todorov, and D. Dundas, *Phys. Rev. B* **85**, 245444 (2012).
  - [4] T. N. Todorov, D. Dundas, A. T. Paxton, and A. P. Horsfield, *Beilstein J. Nanotechnol.* **2**, 727 (2011).
  - [5] T. N. Todorov, B. Cunningham, D. Dundas, and A. P. Horsfield, *Mater. Sci. Technol.* **33**, 1442 (2017).
  - [6] M. Stamenova, S. Sanvito, and T. Todorov, *Phys. Rev. B* **72**, 134407 (2005).
  - [7] X. Zhang, C. Zhang, C. Sun, X. Xu, L. Du, J. Tao, and J. Zhao, *AIP Advances* **11**, 075225 (2021).
  - [8] X. Wang, G. Guo, Y. Nie, G. Zhang, and Z. Li, *Phys. Rev. B* **86**, 054445 (2012).
  - [9] T. N. Todorov, D. Dundas, J.-T. Lü, M. Brandbyge, and P. Hedegård, *Eur. J. Phys.* **35**, 065004 (2014).
  - [10] E. J. McEniry, D. R. Bowler, D. Dundas, A. P. Horsfield, C. G. Sánchez, and T. N. Todorov, *J. Phys.: Condens. Matter* **19**, 196201 (2007).
  - [11] V. Rizzi, T. N. Todorov, J. J. Kohanoff, and A. A. Correa, *Phys. Rev. B* **93**, 024306 (2016).
  - [12] J.-T. Lü, P. Hedegård, and M. Brandbyge, *Phys. Rev. Lett.* **107**, 046801 (2011).
  - [13] R. J. Preston, T. D. Honeychurch, and D. S. Kosov, *Phys. Rev. B* **106**, 195406 (2022).
  - [14] D. Dundas, E. J. McEniry, and T. N. Todorov, *Nat. Nanotechnol.* **4**, 99 (2009).
  - [15] J.-T. Lü, M. Brandbyge, and P. Hedegård, *Nano Lett.* **10**, 1657 (2010).
  - [16] J.-T. Lü, R. B. Christiansen, J.-S. Wang, P. Hedegård, and M. Brandbyge, *Phys. Rev. Lett.* **114**, 096801 (2015).
  - [17] C. G. Sánchez, M. Stamenova, S. Sanvito, D. R. Bowler, A. P. Horsfield, and T. N. Todorov, *J. Chem. Phys.* **124**, 214708 (2006).
  - [18] A. P. Sutton, T. N. Todorov, M. J. Cawkwell, and J. Hoekstra, *Phil. Mag. B* **81**, 1833 (2001).
  - [19] B. Cunningham, T. N. Todorov, and D. Dundas, *Phys. Rev. B* **90**, 115430 (2014).
  - [20] R. F. L. Evans, P. C. W. J. Fan, T. A. Ostler, M. O. A. Ellis, and R. W. Chantrell, *J. Phys.: Condens. Matter* **26**, 103202 (2014).
  - [21] T. N. Todorov, *J. Phys.: Condens. Matter* **14**, 3049 (2002).
  - [22] H. Funaki and G. Tatara, *Phys. Rev. B* **106**, 134435 (2022).
  - [23] G. Tatara, H. Kohno, and J. Shibata, *Phys. Rep.* **468**, 213 (2008).
  - [24] N. Agrit, C. Untiedt, G. Rubio-Bollinger, and S. Vieira, *Phys. Rev. Lett.* **88**, 216803 (2002).
  - [25] W. Chen, E. Chulkov, and J. Paul, *Phys. Scripta* **54**, 392 (1996).
  - [26] C. Sabater, C. Untiedt, and J. M. van Ruitenbeek, *Beilstein J. Nanotechnol.* **6**, 2338 (2015).